Single- and multi-photon production in e^+e^- collisions at $\sqrt{s}$ up to 209 GeV

A. Heister, S. Schael, R. Barate, R. Bruneliere, I. de Bonis, D. Decamp, C. Goy, S. Jezequel, J P. Lees, Frédérique Martin, et al.

HAL Id: in2p3-00013629
https://hal.in2p3.fr/in2p3-00013629

Submitted on 4 Aug 2003

Single- and multi-photon production
in e^+e^- collisions at $\sqrt{s}$ up to $209\,\mathrm{GeV}$

The ALEPH Collaboration [*])

Abstract

Events containing only energetic photons are analysed in a sample of $628\,\mathrm{pb}^{-1}$ of data recorded from e^+e^- collisions at centre-of-mass energies between 189 and $209\,\mathrm{GeV}$ by the ALEPH detector at LEP. The $e^+e^- \to \nu\bar{\nu}\gamma(\gamma)$ and $e^+e^- \to \gamma\gamma(\gamma)$ cross sections are measured and found to be in agreement with the Standard Model predictions. The number of light neutrino generations is determined to be $N_\nu = 2.86 \pm 0.09$. Upper limits are derived on the cross sections for photon production in the context of several supersymmetric models. Limits are also set on the parameters of models with extra spatial dimensions, with contact interactions and with excited electrons.

(Submitted to the European Physical Journal C)

---

[*]) See next pages for the list of authors.

The ALEPH Collaboration

A. Heister, S. Schael

Physikalisches Institut das RWTH-Aachen, D-52056 Aachen, Germany

R. Barate, R. Brunelière, I. De Bonis, D. Decamp, C. Goy, S. Jezequel, J.-P. Lees, F. Martin, E. Merle, M.-N. Minard, B. Pietrzyk, B. Trocmé

Laboratoire de Physique des Particules (LAPP), IN²P³-CNRS, F-74019 Annecy-le-Vieux Cedex, France

G. Boix,[25] S. Bravo, M.P. Casado, M. Chmeissani, J.M. Crespo, E. Fernandez, M. Fernandez-Bosman, Ll. Garrido,[15] E. Graugés, J. Lopez, M. Martinez, G. Merino, Ll.M. Mir,[4] A. Pacheco, D. Paneque, H. Ruiz

Institut de Física d'Altes Energies, Universitat Autònoma de Barcelona, E-08193 Bellaterra (Barcelona), Spain[7]

A. Colaleo, D. Creanza, N. De Filippis, M. de Palma, G. Iaselli, G. Maggi, M. Maggi, S. Nuzzo, A. Ranieri, G. Raso,[24] F. Ruggieri, G. Selvaggi, L. Silvestris, P. Tempesta, A. Tricomi,[3] G. Zito

Dipartimento di Fisica, INFN Sezione di Bari, I-70126 Bari, Italy

X. Huang, J. Lin, Q. Ouyang, T. Wang, Y. Xie, R. Xu, S. Xue, J. Zhang, L. Zhang, W. Zhao

Institute of High Energy Physics, Academia Sinica, Beijing, The People's Republic of China[8]

D. Abbaneo, P. Azzurri, T. Barklow,[30] O. Buchmüller,[30] M. Cattaneo, F. Cerutti, B. Clerbaux,[34] H. Drevermann, R.W. Forty, M. Frank, F. Gianotti, T.C. Greening,[26] J.B. Hansen, J. Harvey, D.E. Hutchcroft, P. Janot, B. Jost, M. Kado,[2] P. Mato, A. Moutoussi, F. Ranjard, L. Rolandi, D. Schlatter, G. Sguazzoni, W. Tejessy, F. Teubert, A. Valassi, I. Videau, J.J. Ward

European Laboratory for Particle Physics (CERN), CH-1211 Geneva 23, Switzerland

F. Badaud, S. Dessagne, A. Falvard,[20] D. Fayolle, P. Gay, J. Jousset, B. Michel, S. Monteil, D. Pallin, J.M. Pascolo, P. Perret

Laboratoire de Physique Corpusculaire, Université Blaise Pascal, IN²P³-CNRS, Clermont-Ferrand, F-63177 Aubière, France

J.D. Hansen, J.R. Hansen, P.H. Hansen, B.S. Nilsson

Niels Bohr Institute, 2100 Copenhagen, DK-Denmark[9]

A. Kyriakis, C. Markou, E. Simopoulou, A. Vayaki, K. Zachariadou

Nuclear Research Center Demokritos (NRCD), GR-15310 Attiki, Greece

A. Blondel,[12] J.-C. Brient, F. Machefert, A. Rougé, M. Swynghedauw, R. Tanaka H. Videau

Laboratoire de Physique Nucléaire et des Hautes Energies, Ecole Polytechnique, IN²P³-CNRS, F-91128 Palaiseau Cedex, France

V. Ciulli, E. Focardi, G. Parrini

Dipartimento di Fisica, Università di Firenze, INFN Sezione di Firenze, I-50125 Firenze, Italy

A. Antonelli, M. Antonelli, G. Bencivenni, F. Bossi, G. Capon, V. Chiarella, P. Laurelli, G. Mannocchi,[5] G.P. Murtas, L. Passalacqua

Laboratori Nazionali dell'INFN (LNF-INFN), I-00044 Frascati, Italy

J. Kennedy, J.G. Lynch, P. Negus, V. O'Shea, A.S. Thompson

Department of Physics and Astronomy, University of Glasgow, Glasgow G12 8QQ,United Kingdom[10]

S. Wasserbaech

    Department of Physics, Haverford College, Haverford, PA 19041-1392, U.S.A.

R. Cavanaugh,[33] S. Dhamotharan,[21] C. Geweniger, P. Hanke, V. Hepp, E.E. Kluge, G. Leibenguth, A. Putzer, H. Stenzel, K. Tittel, M. Wunsch[19]

    Kirchhoff-Institut für Physik, Universität Heidelberg, D-69120 Heidelberg, Germany[16]

R. Beuselinck, W. Cameron, G. Davies, P.J. Dornan, M. Girone,[1] R.D. Hill, N. Marinelli, J. Nowell, S.A. Rutherford, J.K. Sedgbeer, J.C. Thompson,[14] R. White

    Department of Physics, Imperial College, London SW7 2BZ, United Kingdom[10]

V.M. Ghete, P. Girtler, E. Kneringer, D. Kuhn, G. Rudolph

    Institut für Experimentalphysik, Universität Innsbruck, A-6020 Innsbruck, Austria[18]

E. Bouhova-Thacker, C.K. Bowdery, D.P. Clarke, G. Ellis, A.J. Finch, F. Foster, G. Hughes, R.W.L. Jones, M.R. Pearson, N.A. Robertson, M. Smizanska

    Department of Physics, University of Lancaster, Lancaster LA1 4YB, United Kingdom[10]

O. van der Aa, C. Delaere, V. Lemaitre

    Institut de Physique Nucléaire, Département de Physique, Université Catholique de Louvain, 1348 Louvain-la-Neuve, Belgium

U. Blumenschein, F. Hölldorfer, K. Jakobs, F. Kayser, K. Kleinknecht, A.-S. Müller, G. Quast,[6] B. Renk, H.-G. Sander, S. Schmeling, H. Wachsmuth, C. Zeitnitz, T. Ziegler

    Institut für Physik, Universität Mainz, D-55099 Mainz, Germany[16]

A. Bonissent, P. Coyle, C. Curtil, A. Ealet, D. Fouchez, P. Payre, A. Tilquin

    Centre de Physique des Particules de Marseille, Univ Méditerranée, IN^2P^3-CNRS, F-13288 Marseille, France

F. Ragusa

    Dipartimento di Fisica, Università di Milano e INFN Sezione di Milano, I-20133 Milano, Italy.

A. David, H. Dietl, G. Ganis,[27] K. Hüttmann, G. Lütjens, W. Männer, H.-G. Moser, R. Settles, G. Wolf

    Max-Planck-Institut für Physik, Werner-Heisenberg-Institut, D-80805 München, Germany[16]

J. Boucrot, O. Callot, M. Davier, L. Duflot, J.-F. Grivaz, Ph. Heusse, A. Jacholkowska,[32] L. Serin, J.-J. Veillet, J.-B. de Vivie de Régie,[28] C. Yuan

    Laboratoire de l'Accélérateur Linéaire, Université de Paris-Sud, IN^2P^3-CNRS, F-91898 Orsay Cedex, France

G. Bagliesi, T. Boccali, L. Foà, A. Giammanco, A. Giassi, F. Ligabue, A. Messineo, F. Palla, G. Sanguinetti, A. Sciabà, R. Tenchini,[1] A. Venturi,[1] P.G. Verdini

    Dipartimento di Fisica dell'Università, INFN Sezione di Pisa, e Scuola Normale Superiore, I-56010 Pisa, Italy

O. Awunor, G.A. Blair, G. Cowan, A. Garcia-Bellido, M.G. Green, L.T. Jones, T. Medcalf, A. Misiejuk, J.A. Strong, P. Teixeira-Dias

    Department of Physics, Royal Holloway & Bedford New College, University of London, Egham, Surrey TW20 OEX, United Kingdom[10]

R.W. Clifft, T.R. Edgecock, P.R. Norton, I.R. Tomalin

    Particle Physics Dept., Rutherford Appleton Laboratory, Chilton, Didcot, Oxon OX11 OQX, United Kingdom[10]

B. Bloch-Devaux, D. Boumediene, P. Colas, B. Fabbro, E. Lançon, M.-C. Lemaire, E. Locci, P. Perez, J. Rander, B. Tuchming, B. Vallage

    CEA, DAPNIA/Service de Physique des Particules, CE-Saclay, F-91191 Gif-sur-Yvette Cedex, France[17]

N. Konstantinidis, A.M. Litke, C. Loomis,[35] G. Taylor

    Institute for Particle Physics, University of California at Santa Cruz, Santa Cruz, CA 95064, USA[22]

C.N. Booth, S. Cartwright, F. Combley,[31] P.N. Hodgson, M. Lehto, L.F. Thompson

Department of Physics, University of Sheffield, Sheffield S3 7RH, United Kingdom[10]

K. Affholderbach,[23] A. Böhrer, S. Brandt, C. Grupen, J. Hess, A. Ngac, G. Prange, U. Sieler

Fachbereich Physik, Universität Siegen, D-57068 Siegen, Germany[16]

C. Borean, G. Giannini

Dipartimento di Fisica, Università di Trieste e INFN Sezione di Trieste, I-34127 Trieste, Italy

H. He, J. Putz, J. Rothberg

Experimental Elementary Particle Physics, University of Washington, Seattle, WA 98195 U.S.A.

S.R. Armstrong, K. Berkelman, K. Cranmer, D.P.S. Ferguson, Y. Gao,[29] S. González, O.J. Hayes, H. Hu, S. Jin, J. Kile, P.A. McNamara III, J. Nielsen, Y.B. Pan, J.H. von Wimmersperg-Toeller, W. Wiedenmann, J. Wu, Sau Lan Wu, X. Wu, G. Zobernig

Department of Physics, University of Wisconsin, Madison, WI 53706, USA[11]

G. Dissertori

Institute for Particle Physics, ETH Hönggerberg, 8093 Zürich, Switzerland.

1 Introduction

In high-energy electron-positron annihilations, the dominant Standard Model (SM) contributions to events in which the only detectable final-state particles are photons come from the electroweak process $e^+e^- \to \nu\bar{\nu}\gamma(\gamma)$ and the QED process $e^+e^- \to \gamma\gamma(\gamma)$. The former is dominated by the reaction $e^+e^- \to \gamma(\gamma)Z$, with $Z \to \nu\bar{\nu}$. An additional contribution arises from t-channel W exchange with one or more photons radiated from the incoming $e^\pm$ or from the virtual W. This process leads to a final state with one or more detected photons accompanied by significant missing energy, missing momentum, and missing mass. It has been extensively studied at LEP at lower energies [1, 2, 3]. In the SM framework, the reaction $e^+e^- \to \gamma\gamma(\gamma)$ proceeds via t-channel electron exchange. The resulting experimental signature is two coplanar, energetic photons. This process has been previously studied at LEP as described in [1–4].

New physics processes can also lead to the final-state topologies described above. This is possible in the context of various supersymmetric (SUSY) models, including the Minimal Supersymmetric extension of the Standard Model (MSSM) [5], Gauge Mediated Supersymmetry Breaking (GMSB) theories [6] and scenarios with a super-light gravitino [7], and in theories with TeV-scale quantum gravity [8], with contact interactions [9] and with excited electrons [10, 11].

This paper reports on a study of photonic final states with the ALEPH detector at LEP, at the highest available e^+e^- centre-of-mass energies. The data cover $\sqrt{s}$ between 189 and 209 GeV, with a total integrated luminosity of $628\,\text{pb}^{-1}$, as detailed in Table 1.

Table 1: *The range of centre-of-mass energies, the corresponding average and the integrated luminosities for the data samples used in the analyses.*

Range of $\sqrt{s}$ (GeV)	188.6	191.6	195.5	199.5	201.6	203.0–205.5	205.5–209.0
Average $\sqrt{s}$ (GeV)	188.6	191.6	195.5	199.5	201.6	205.0	206.7
Int. luminosity (pb^{-1})	173.6	28.9	79.9	87.0	44.4	79.5	134.3

This paper is organized as follows. After a brief description of the ALEPH detector and photon identification in Section 2, the simulated data samples used for the analyses are described in Section 3. The selection of events with one photon and missing energy, the measurements of the $e^+e^- \to \nu\bar{\nu}\gamma(\gamma)$ cross section and of the number of light neutrino generations, and searches for new physics in the single-photon topology are discussed in Section 4. Searches for new physics in events with two or more photons and missing energy are presented in Section 5. The selection of events with two hard collinear photons, the measurement of the $e^+e^- \to \gamma\gamma(\gamma)$ cross section and the corresponding searches for new physics processes are described in Section 6. Conclusions are presented in Section 7.

2 The ALEPH detector and photon identification

The ALEPH detector and its performance are described in detail in Refs. [12, 13]. The analysis presented here depends largely on the performance of the electromagnetic calorimeter (ECAL).

The ECAL is a lead/wire-chamber sampling calorimeter consisting of 36 modules, twelve in the barrel and twelve in each endcap, which provide coverage in the angular range $|\cos\theta| < 0.98$. Cathode pads associated with each layer of the wire chambers are connected to form projective towers, each subtending approximately $0.9° \times 0.9°$, read out in three segments in depth ("storeys"). This high granularity provides excellent identification of photons and electrons. The energy calibration of the ECAL is obtained from Bhabha events, $e^+e^- \to \gamma\gamma$ events and events from two-photon interactions, $\gamma\gamma \to e^+e^-$. The energy resolution for isolated photons is $\sigma(E)/E = 0.18/\sqrt{E} + 0.009$ (E in GeV). The ECAL also provides a measurement of the event time t_0 relative to the beam crossing with a resolution of better than $15\,\mathrm{ns}$ for showers with energy greater than $1\,\mathrm{GeV}$.

The hadron calorimeter (HCAL) and the luminosity calorimeters extend the coverage to $34\,\mathrm{mrad}$ from the beam axis. Together with the external muon chambers, they are used in this analysis mainly to veto events in which photons are accompanied by other energetic particles. The tracking system provides efficient reconstruction of isolated charged particles in the angular range $|\cos\theta| < 0.95$.

Photon candidates are identified by an algorithm [13] which performs a topological search for localized energy deposits within groups of neighbouring ECAL towers. Photon candidates may also be identified [13] if they convert in the material of the tracking system, which amounts to 6% of a radiation length at normal incidence.

The trigger most relevant for photon events is the neutral-energy trigger with a threshold of 1 GeV (2.3 GeV) in any ECAL barrel (endcap) module. The trigger efficiency for the selections described below is estimated to be at least 99.8%.

3   Simulation programs

The measurements of the $e^+e^- \to \nu\bar{\nu}\gamma(\gamma)$ cross section and of the number of light neutrino families are based on efficiencies estimated with the KK generator [14]. This generator is also used to evaluate the SM background for the searches for new physics in the photon(s) plus missing energy channels. The KK program uses the YFS [15] approach to generate an arbitrary number of initial-state-radiation photons. It includes the effects of photons radiated from exchanged virtual W's. The predictions of KK are checked by comparison with an independent generator, NUNUGPV [16], which is based on exact lowest-order amplitudes for the production of up to three photons in the final state, modified for higher-order QED effects using transverse momentum dependent structure functions. The contribution of missing higher-order electroweak corrections, which are not treated by either generator, is estimated to be smaller than 1% [17].

The experimental efficiency for the reaction $e^+e^- \to \gamma\gamma(\gamma)$ is obtained with the GGG generator [18], which includes all contributions to order α^3. Events with four hard photons observed in the detector are simulated by an order α^4 generator [19].

The efficiencies for the processes $e^+e^- \to XX$ and $e^+e^- \to XY$ with $X \to Y\gamma$, where Y is invisible, are estimated with SUSYGEN [20] assuming isotropic production and decay of X and taking into account the effects of initial-state radiation (ISR) [21]. The background from

Bhabha scattering where initial- or final-state particles radiate a photon is studied with the BHWIDE [22] generator.

4   One photon and missing energy

4.1   Event selection

The acceptance region for single photon and missing energy events is defined to be $|\cos\theta| < 0.95$ with $p_\perp > 0.0375\sqrt{s}$, where θ is the polar angle of the photon relative to the beam line, and $p_\perp$ is the photon transverse momentum. The basic selection cuts are designed to reduce background from radiative Bhabha events ($\mathrm{e^+e^-} \to \mathrm{e^+e^-}\gamma$). There must be one and only one photon within the acceptance region, no charged particle tracks (except those from an identified photon conversion), no energy deposited within $14°$ of the beam axis, and less than $1\,\mathrm{GeV}$ of additional visible energy. To reduce cosmic-ray background and to remove the few events with detector noise in the ECAL, cuts are applied on the number of hits in the outer part of the HCAL, and the event time, as measured in the ECAL, is required to be consistent with the beam crossing. Furthermore, the photon candidate must have a small "impact parameter" [1], consistent with the photon originating from the interaction region, and a compact shower development in the ECAL [1].

4.2   Measurement of the $\mathrm{e^+e^-} \to \nu\bar{\nu}\gamma(\gamma)$ cross section and the number of light neutrino generations

The efficiency of the above selection for the process $\mathrm{e^+e^-} \to \nu\bar{\nu}\gamma(\gamma)$ is 86%, independent of $\sqrt{s}$. An additional efficiency loss is due to beam-related background and uncorrelated noise in the detector; it varies in the range 3–6%, depending on the centre-of-mass energy, and is estimated from events triggered on random beam crossings. The numbers of selected single-photon events, the numbers of events expected from the KK simulation, and the measured cross sections are summarized in Table 2, for the different centre-of-mass energies. The systematic uncertainties on the measured cross sections are listed in Table 3; the individual contributions are described in Ref. [1]. All the listed uncertainties, except that related to the statistics of the simulation, are common for all centre-of-mass energies.

The ratio of the measured to expected cross section is shown in Fig. 1 as a function of $\sqrt{s}$. The event missing mass and the photon $|\cos\theta|$ distributions for the selected events, summing the contributions for all values of $\sqrt{s}$ between 189 and $209\,\mathrm{GeV}$, are shown in Fig. 2. The data agree with the SM expectations and are used to constrain new physics processes in the following sections.

If additional generations of light neutrinos exist beyond ν_e, ν_μ and ν_τ, they contribute to the spectra in Fig. 2. To explore this possibility, a two-dimensional binned maximum likelihood fit is performed for the number of light neutrino generations, N_ν, to the missing mass versus photon polar angle distribution for the observed events. The expected distribution is generated with the KK Monte Carlo assuming all neutrino generations have universal couplings and negligible

Table 2: *Observed and expected numbers of single-photon events and measured cross section for the different centre-of-mass energies. The measured cross sections correspond to one and only one photon detected in the acceptance region $|\cos\theta| < 0.95$ and $p_\perp > 0.0375\sqrt{s}$. The uncertainties quoted on the cross-section measurements are only statistical.*

$\sqrt{s}$ (GeV)	Events observed	Events expected	Measured cross section (pb)
189	484	493	3.43 ± 0.16
192	81	76	3.47 ± 0.39
196	197	212	3.03 ± 0.22
200	231	221	3.23 ± 0.21
202	110	111	2.99 ± 0.29
205	182	190	2.84 ± 0.21
207	292	306	2.67 ± 0.16
189–207	1577	1610	

Table 3: *Systematic uncertainties on the measured cross section for single-photon production.*

Source	Uncertainty (%)
Photon selection	0.6
Converted photon selection	0.3
Background	<0.1
Integrated luminosity	0.5
Monte Carlo theory	1.5
Monte Carlo statistics	0.5
Total (in quadrature)	1.8

mass. The centre-of-mass energy dependence of the cross section and the 1.8% total systematic error reported in Table 3 are taken into account in the fit. The result, $N_\nu = 2.86 \pm 0.09$, is consistent with three light neutrino generations, and rules out $N_\nu = 2$ and $N_\nu = 4$ at the 9 and 12 σ levels, respectively. This result has a precision comparable to that of earlier results based on the same technique [3] and has systematic uncertainties different from those of the more precise measurement based on the Z lineshape [23]. The experimental missing mass distribution is shown in Fig. 3 together with the result of the fit and with the expected distributions for $N_\nu = 2$ and $N_\nu = 4$.

4.3 Search for $e^+e^- \to XY \to YY\gamma$

Search results are given here for the generic process $e^+e^- \to XY$, followed by the radiative decay $X \to Y\gamma$, leading to a $YY\gamma$ final state where Y escapes direct detection. Examples of such processes would be $e^+e^- \to \chi_2^0\chi_1^0 \to \chi_1^0\chi_1^0\gamma$ in the MSSM [5], where χ_1^0 and χ_2^0 are the lightest and next-to-lightest neutralinos, respectively, and $e^+e^- \to \chi_1^0\tilde{G} \to \tilde{G}\tilde{G}\gamma$ in GMSB [24],

4

where the gravitino $\tilde{G}$ and the neutralino χ_1^0 are the lightest and next-to-lightest SUSY particles, respectively.

A fit to the single-photon plus missing energy events is carried out as above under the hypothesis that the data includes a mixture of signal from $e^+e^- \to XY \to YY\gamma$ plus SM background from $e^+e^- \to \nu\bar{\nu}\gamma(\gamma)$. The fit is performed for all possible X,Y mass combinations in steps of $1\,\text{GeV}/c^2$. The results are shown in Fig. 4 as 95% confidence level (C.L.) upper limits on the $e^+e^- \to XY$ production cross section, assuming an $X \to Y\gamma$ branching ratio of 100% and a negligible X lifetime. These results are valid at $\sqrt{s} = 207\,\text{GeV}$; data recorded at lower centre-of-mass energies are included with a β/s cross-section dependence.

4.4   Search for super-light gravitinos

In SUSY models with a super-light gravitino $\tilde{G}$ and all other supersymmetric particles too heavy to be produced at LEP [7], it may still be possible to discover SUSY via the reaction $e^+e^- \to \tilde{G}\tilde{G}\gamma$. As the cross section is proportional to $1/M_{\tilde{G}}^4$ (where $M_{\tilde{G}}$ is the gravitino mass), the process $e^+e^- \to \tilde{G}\tilde{G}\gamma$ can become observable for sufficiently low values of $M_{\tilde{G}}$. Alternatively, in the absence of a signal, an upper limit on the cross section can be translated into a lower limit on $M_{\tilde{G}}$.

A fit is performed as above for a signal, calculated from the differential cross section given in Ref. [7], on top of the SM background. From the fit, a cross-section upper limit of $0.13\,\text{pb}$ at $\sqrt{s} = 207\,\text{GeV}$ is obtained at 95% C.L., which in turn provides a 95% C.L. lower limit of $1.3 \times 10^{-5}\ \text{eV}/c^2$ for the gravitino mass.

4.5   Search for TeV-scale quantum gravity

In theories of TeV-scale quantum gravity as proposed in Ref. [8], gravity can propagate in extra spatial dimensions. One of the possible consequences is that a spectrum of massive gravitons G could be produced in association with a photon in e^+e^- annihilations. The gravitons, which have interactions of gravitational strength and very large lifetime, escape direct detection. Consequently, their production should give rise to an excess of events in the single-photon plus missing energy channel.

The differential cross section for the process $e^+e^- \to G\gamma$ depends on both the gravity scale M_D and the number of extra dimensions δ, and is given by [25]

$$\frac{d^2\sigma}{dx\,d\cos\theta} = \frac{\alpha}{32s}\frac{\pi^{\delta/2}}{\Gamma(\delta/2)}\left(\frac{\sqrt{s}}{M_\text{D}}\right)^{\delta+2} f(x,\cos\theta),$$

with

$$f(x,\cos\theta) = \frac{2(1-x)^{\frac{\delta}{2}-1}}{x(1-\cos^2\theta)}[(2-x)^2(1-x+x^2) - 3x^2(1-x)\cos^2\theta - x^4\cos^4\theta],$$

where x is the ratio of the photon energy to the beam energy, and θ is the polar angle of the photon.

5

Limits on the parameter M_{D} as a function of the number of extra dimensions are derived from a fit, of the type described above, performed under the hypothesis that the data contains a mixture of signal (calculated with the cross section given above) and SM background. Initial-state radiation is taken into account [21]. The fit parameter is taken to be $(1/M_{\mathrm{D}})^{\delta+2}$. The fit results are displayed in Table 4. No statistically significant signal is observed, and 95% C.L. lower limits $M_{\mathrm{D}95}$ are placed on the gravity scale M_{D} as a function of δ. These limits are shown in Table 4 along with the corresponding upper limits R_{95} on the size R of the extra spatial dimensions, derived from the relation

$$G_N^{-1} = 8\pi R^\delta M_{\mathrm{D}}^{2+\delta},$$

where G_N is the Newtonian gravitational constant.

Table 4: *Fitted values for $(1/M_D)^{\delta+2}$, the lower limits M_{D95} on the gravity scale M_D, and the upper limits R_{95} on the size R of the extra dimensions, as a function of the number of extra dimensions δ. All the limits are at 95% C.L.*

δ	$(1/M_{\mathrm{D}})^{\delta+2}$	$M_{\mathrm{D}95}$ (TeV)	R_{95} (cm)
2	$0.06 \pm 0.18\,\mathrm{TeV}^{-4}$	1.26	3.0×10^{-2}
3	$0.30 \pm 0.54\,\mathrm{TeV}^{-5}$	0.95	3.9×10^{-7}
4	$1.1 \pm 2.0\,\mathrm{TeV}^{-6}$	0.77	1.4×10^{-9}
5	$4.5 \pm 8.4\,\mathrm{TeV}^{-7}$	0.65	5.1×10^{-11}
6	$18 \pm 40\,\mathrm{TeV}^{-8}$	0.57	5.6×10^{-12}

4.6 Search for $\mathrm{e^+e^-} \to \chi_1^0\chi_1^0 \to \tilde{\mathrm{G}}\tilde{\mathrm{G}}\gamma\gamma$ with intermediate χ_1^0 lifetime

In GMSB models where χ_1^0 is the next-to-lightest SUSY particle, the neutralino can have a non-negligible lifetime, depending on the gravitino mass. A dedicated analysis was developed [26] to search for events from the reaction $\mathrm{e^+e^-} \to \chi_1^0\chi_1^0 \to \tilde{\mathrm{G}}\tilde{\mathrm{G}}\gamma\gamma$, in which one neutralino decays within the volume bounded by the ECAL, while the other decays outside the detector. The event signature is a single photon plus missing energy, but the photon does not point back to the interaction region. The basic event selection criteria are the same as those described in Section 4.1, except that the cut on the photon shower compactness is not applied and the photon impact parameter is required to be greater than 40 cm, which is inconsistent with the photon originating from the interaction region. In addition, the event must have no converted photons.

To further reduce background from cosmic rays, penetrating muons produced by upstream interactions of the LEP beams with matter, and detector noise in the ECAL, additional cuts are imposed as follows. At least 40% of the photon energy must be recorded in the ECAL; there must be no more than 50 fired storeys, in addition to those associated with the photon, in any one ECAL module; and there must be no activity in either the muon chambers or the ECAL within a transverse distance of 15 cm from the photon candidate.

6

The efficiency of this selection depends on the neutralino decay length in the laboratory frame, and has a maximum value of 10% for decay lengths of around 8 m [26]. After all cuts, two events are selected in the data. The background from $e^+e^- \to \nu\bar{\nu}\gamma(\gamma)$ is estimated to be 0.8 events. The background from cosmic rays, beam muons and detector noise is estimated to be 0.2 ± 0.2 events. Under the assumptions of the Minimal Gauge-mediated Model (MGM) [27], discussed in Section 5.2, a limit on the mass of χ_1^0 as a function of the χ_1^0 proper lifetime is computed. The excluded region is shown in Fig. 5, along with the region excluded by the analysis discussed in Section 5.2.

5 Two or more photons and missing energy

5.1 Event selection

The preselection is designed to select events with acoplanar photons and to reduce the background from $e^+e^- \to \gamma\gamma(\gamma)$ and doubly-radiative Bhabha events ($e^+e^- \to e^+e^-\gamma\gamma$). There must be at least two photons, each with energy larger than $1\,\mathrm{GeV}$, within the acceptance region $|\cos\theta| < 0.95$. There must be no charged particle tracks (except those coming from an identified photon conversion) and less than $1\,\mathrm{GeV}$ of non-photonic additional visible energy. The acoplanarity angle of the two most energetic photons must be smaller than 177°, and the total transverse momentum of the multi-photon system must be greater than 3.75% of the missing energy. Events with more than two photons are required to have a missing energy larger than $0.4\sqrt{s}$.

When this selection is applied to the 189–209 GeV data, 93 events are selected, while 88 are predicted from the process $e^+e^- \to \nu\bar{\nu}\gamma\gamma(\gamma)$. From a comparison of different event generators [14, 16], the theoretical uncertainty on this prediction, including the effect of missing higher-order electroweak diagrams, is estimated to be less than 5%. The missing mass distribution and the energy distribution of the second most energetic photon for the selected data events are compared in Fig. 6 to the SM expectations.

5.2 Search for $e^+e^- \to \chi_1^0\chi_1^0 \to \tilde{G}\tilde{G}\gamma\gamma$

The GMSB process $e^+e^- \to \chi_1^0\chi_1^0 \to \tilde{G}\tilde{G}\gamma\gamma$ gives rise to final states with two acoplanar photons for small neutralino lifetimes. As the gravitino is nearly massless, and the decay $\chi_1^0 \to \tilde{G}\gamma$ is isotropic in the χ_1^0 rest frame, the photon energy spectrum is expected to be flat. A threshold cut on the energy of the second most energetic photon is therefore very effective at reducing the SM background, where this photon is predominantly produced via bremsstrahlung. The optimization of the threshold cut was done in the context of the MGM [27]. In this model the lightest neutralino is pure bino, and the right-handed selectron (left-handed selectron) mass is 1.1 (2.5) times the neutralino mass. At LEP, the production of bino-like neutralino pairs proceeds via t-channel selectron exchange, with right-handed selectron exchange dominating over left-handed selectron exchange. Within this framework, the optimized value for the threshold cut is 37 GeV. Four candidate events are selected in the data, with 4.9 expected

7

from background.

The 95% C.L. upper limit on the $e^+e^- \to \chi_1^0\chi_1^0$ production cross section at $\sqrt{s} = 207\,\text{GeV}$, obtained after subtraction of the expected background, is shown in Fig. 7 for a $\chi_1^0 \to \gamma\tilde{G}$ branching ratio of 100% and a χ_1^0 laboratory lifetime of less than 3 ns. The data collected at lower centre-of-mass energies are included by scaling their luminosities according to the cross-section predictions of the MGM. The systematic uncertainty for this analysis is dominated by that on the photon reconstruction efficiency, estimated to be smaller than 2%, and that on the level of background from standard processes, estimated to be 10%. The effect of these uncertainties on the cross-section upper limit, taken into account by means of the method of Ref. [28], is less than 1%. The $e^+e^- \to \chi_1^0\chi_1^0$ cross section in the MGM is also shown in Fig. 7. The neutralino mass limit obtained for this model is $M_{\chi_1^0} \geq 98.8\,\text{GeV}/c^2$ at 95% C.L. The effect of the systematic uncertainties on the mass limit is negligible.

The χ_1^0 mass limit as a function of the χ_1^0 proper lifetime is shown in Fig. 5, together with the single-photon results described in Section 4.6.

The excluded region in the χ_1^0-$\tilde{e}_R$ mass plane, obtained after relaxing the mass relations of the MGM, is shown in Fig. 8. The region where the properties of the CDF event described in [29] are consistent with the process $q\bar{q} \to \tilde{e}_R\tilde{e}_R \to ee\chi_1^0\chi_1^0 \to ee\tilde{G}\tilde{G}\gamma\gamma$ [30] is also shown. Almost the entire region favoured by the CDF event is excluded at 95% C.L. by this analysis.

These results, together with those of Section 4.6, are interpreted in a more general GMSB framework in Ref. [31].

5.3   Search for $e^+e^- \to XX \to YY\gamma\gamma$

In the general case where Y is massive and the X-Y mass difference may therefore be small, as could be the case for the MSSM process $e^+e^- \to \chi_2^0\chi_2^0 \to \chi_1^0\chi_1^0\gamma\gamma$, the photon energies may be low. A threshold energy cut of 37 GeV, as used in the analysis described in Section 5.2, is therefore not appropriate. The selection is designed to reduce the dominant background from $e^+e^- \to \nu\bar{\nu}\gamma\gamma(\gamma)$, characterized by a missing mass M_{miss} near the Z mass and one or more photons at small angles relative to the beam axis and/or with low energies. It is therefore required that $M_{\text{miss}} < 82\,\text{GeV}/c^2$, or $M_{\text{miss}} > 100\,\text{GeV}/c^2$, or the energy of the second most energetic photon be greater than 10 GeV. Furthermore, each of the two most energetic photons must have $|\cos\theta| < 0.81$.

When this selection is applied to the data, 26 events are selected, with 28 events expected from the $e^+e^- \to \nu\bar{\nu}\gamma\gamma(\gamma)$ process. The resulting cross-section upper limit is shown in Fig. 9, as a function of the masses of X and Y, assuming a X laboratory lifetime of less than 3 ns. This limit is derived without performing background subtraction, but the observed candidates are taken into account only where they are kinematically consistent with a given X, Y mass pairing. The limits are established at $\sqrt{s} = 207\,\text{GeV}$; lower-energy data are taken into account with a β/s threshold dependence. The systematic uncertainty on the efficiency of this selection is estimated to be smaller than 2%, and the resulting effect on the cross-section upper limits is also smaller than 2%.

6 Hard collinear photon pairs

6.1 Event selection

Events with collinear energetic photons are selected by requiring that there be at least two photons, each with energy above $0.25\sqrt{s}$ and within the acceptance region $|\cos\theta| < 0.95$, and that the angle between the two most energetic photons be at least 160°. To reduce the background from Bhabha scattering, it is further required that there be no charged particle tracks in the event (except those from an identified photon conversion) and that there be at most one converted photon. Cosmic rays that traverse the detector are eliminated by requiring no hits in the outer part of the HCAL and that the measured interaction time in ECAL be consistent with the beam crossing time.

The efficiency of this selection for the process $e^+e^- \to \gamma\gamma(\gamma)$ is 84%, independent of centre-of-mass energy. The numbers of events observed and expected after the above selection at the different centre-of-mass energies are given in Table 5. A total of 4353 events are observed in the data, compared with a SM expectation of 4582 events.

Table 5: *Observed and expected numbers of collinear photon events and measured $e^+e^- \to \gamma\gamma$ cross section for the different centre-of-mass energies. The uncertainties quoted on the cross-section measurements are only statistical.*

$\sqrt{s}$ (GeV)	Events observed	Events expected	Measured cross section (pb)
189	1309	1402	9.29 ± 0.26
192	208	220	9.12 ± 0.63
196	570	587	9.00 ± 0.38
200	603	620	8.65 ± 0.35
202	311	306	8.85 ± 0.50
205	485	540	7.57 ± 0.34
207	867	906	7.93 ± 0.27
189–207	4353	4582	

6.2 Measurement of the $e^+e^- \to \gamma\gamma(\gamma)$ cross section

The lowest-order (Born) differential cross section for electron-positron annihilation into two photons is given by

$$\left(\frac{d\sigma}{d\Omega}\right)_{\text{Born}} = \frac{\alpha^2}{s}\left(\frac{1 + \cos^2\theta}{1 - \cos^2\theta}\right).$$

The observed cross section is modified, relative to the Born-level prediction, by higher-order radiative effects (particularly ISR), as well as effects due to detector resolution and efficiency.

Due to ISR, the centre-of-mass frame of the two detected photons is not, in general, at rest in the laboratory. The events are therefore transformed into the two-photon rest frame to define the production angle θ^* [1]. The measured and expected distributions of this production angle, summed over data taken with $\sqrt{s}$ between 189 and 209 GeV, are shown in Fig. 10.

The measured cross sections for events inside the acceptance region defined by $|\cos\theta^*| < 0.95$ are given, for each centre-of-mass energy, in Table 5. These measurements are corrected for radiative, as well as detector, effects. They can therefore be compared directly with the Born cross section integrated over the acceptance region. The ratio of observed to Born cross section for the process $e^+e^- \to \gamma\gamma$ is shown in Fig. 11 as a function of centre-of-mass energy.

The systematic uncertainties on these results are listed in Table 6 and described in [1]. The listed errors, except the statistical error from the Monte Carlo samples, are common for all values of $\sqrt{s}$. The individual contributions added in quadrature give a total systematic uncertainty of 2.2%. If both the statistical and systematic uncertainties are taken into account the deficit of observed events represents a 2.1σ effect.

Table 6: *Systematic uncertainties on the $e^+e^- \to \gamma\gamma$ cross-section measurement.*

Source	Uncertainty (%)
Photon selection	1.2
Converted photon selection	0.6
Bhabha background	0.8
Integrated luminosity	0.5
Monte Carlo theory	1.0
Monte Carlo statistics	1.1
Total (in quadrature)	2.2

6.3 Search for TeV-scale quantum gravity

In the framework of quantum gravity [8] mentioned in Section 4.5, the $e^+e^- \to \gamma\gamma$ SM cross section is modified due to additional amplitudes in which a spectrum of virtual gravitons are exchanged in the s channel. The modified cross section is given by [25]

$$\left(\frac{d\sigma}{d\Omega}\right) = \left(\frac{d\sigma}{d\Omega}\right)_{\text{Born}} - \frac{\lambda\alpha s}{2\pi} \left(\frac{1}{M_s^{\pm}}\right)^4 (1 + \cos^2\theta) + \frac{s^3}{16\pi^2} \left(\frac{1}{M_s^{\pm}}\right)^8 (1 - \cos^4\theta),$$

where λ is a phase factor in the interference term which for simplicity is assumed here to take only values of ± 1, and M_s^+ and M_s^- are the corresponding string scale parameters. In the absence of a full theory of quantum gravity, M_s cannot be precisely calculated in terms of the mass scale M_D, but the ratio M_s/M_D is expected to be of order unity.

A binned maximum likelihood fit is performed to the data displayed in Fig. 10 for the parameters $\epsilon_\pm = \pm(1/M_s^\pm)^4$. The systematic uncertainty of 2.2% and the centre-of-mass energy dependence of the cross section are taken into account in the likelihood function. The fit gives

$$\epsilon_\pm = \pm(1/M_s^\pm)^4 = -0.46 \pm 1.10 \text{ TeV}^{-4}.$$

The corresponding 95% C.L. lower limits on M_s^+ and M_s^- are 0.80 TeV and 0.85 TeV, respectively. The ratio of the measured differential cross section to the SM prediction is shown in Fig. 12 as a function of $|\cos\theta^*|$. Also indicated are the predictions with $M_s^\pm$ set to their lower limit values.

6.4 Search for contact interactions

If the electron and photon have non-standard contact interactions of the form eeγ or ee$\gamma\gamma$ in addition to the QED interaction, the differential cross section for $e^+e^- \to \gamma\gamma$ is modified compared to the SM prediction. Three gauge-invariant contact interactions, of dimensionality 6, 7 and 8, are considered [9], and are parameterized by the characteristic mass scales Λ_6, Λ_7 and Λ_8, respectively. The modified differential cross sections can be expressed as

$$\left(\frac{d\sigma}{d\Omega}\right)_6 = \left(\frac{d\sigma}{d\Omega}\right)_{\text{Born}} + \frac{\alpha s}{\Lambda_6^4}(1 + \cos^2\theta),$$

$$\left(\frac{d\sigma}{d\Omega}\right)_7 = \left(\frac{d\sigma}{d\Omega}\right)_{\text{Born}} + \frac{s^2}{32\pi\Lambda_7^6},$$

$$\left(\frac{d\sigma}{d\Omega}\right)_8 = \left(\frac{d\sigma}{d\Omega}\right)_{\text{Born}} + \frac{s^2 m_e^2}{64\pi\Lambda_8^8},$$

where m_e is the electron mass. A fit is performed to the experimental data as described above, yielding the results $1/\Lambda_6^4 = -0.07 \pm 0.18 \text{ TeV}^{-4}$ and $1/\Lambda_7^6 = -1.07 \pm 3.36 \text{ TeV}^{-6}$. Results on Λ_8 are derived from those on Λ_7: $1/\Lambda_8^8 = -8.2 \pm 25.7 \times 10^{12} \text{ TeV}^{-8}$. The corresponding 95% C.L. lower limits on Λ_6, Λ_7 and Λ_8 are 1.35 TeV, 0.74 TeV and 21.4 GeV, respectively.

6.5 Search for excited electrons

An excited electron e*, with a coupling ee*γ, can be exchanged in the t channel of the reaction $e^+e^- \to \gamma\gamma$, and thereby modify the SM differential cross section. For the chiral magnetic coupling of Ref. [10], the differential cross section is [11]

$$\left(\frac{d\sigma}{d\Omega}\right) = \left(\frac{d\sigma}{d\Omega}\right)_{\text{Born}} + \frac{\alpha^2}{4}\frac{f_\gamma^4}{\Lambda^4 M_{e*}^2}\left[\frac{p^4}{(p^2/M_{e*}^2 - 1)^2} + \frac{q^4}{(q^2/M_{e*}^2 - 1)^2} + \frac{\frac{1}{2}s^2\sin^2\theta}{(p^2/M_{e*}^2 - 1)(q^2/M_{e*}^2 - 1)}\right],$$

where f_γ is a dimensionless coupling constant, $p^2 = -\frac{s}{2}(1 - \cos\theta)$, $q^2 = -\frac{s}{2}(1 + \cos\theta)$, M_{e*} is the mass of the excited electron, and Λ represents the compositeness scale. This differential cross section is fitted to the experimental data to determine the parameter $\epsilon = f_\gamma^4/(\Lambda^4 M_{e*}^2)$ for various values of M_{e*}. The results of the fit are summarized in Table 7. For $\Lambda = M_{e*}$ and $f_\gamma = 1$, a 95% C.L. lower limit of 213 GeV/c^2 is obtained on M_{e*}.

11

Table 7: *Fit parameter* $\epsilon = f_\gamma^4/(\Lambda^4 M_{e^*}^2)$, *for various values of* M_{e^*}, *as obtained from a fit to the* $e^+e^- \to \gamma\gamma$ *data.*

M_{e^*} (GeV)	ϵ (TeV)$^{-6}$
200	-1030 ± 6200
300	-930 ± 4080
400	-890 ± 3400
1000	-850 ± 2760
5000	-842 ± 2650

7   Conclusions

Single- and multi-photon production in e^+e^- collisions has been studied with the ALEPH data collected at LEP at centre-of-mass energies between 189 and 209 GeV. The measured cross sections for the processes $e^+e^- \to \nu\bar{\nu}\gamma(\gamma)$ and $e^+e^- \to \gamma\gamma(\gamma)$ are in agreement with the predictions of the Standard Model. The number of light neutrino generations has been measured to be $N_\nu = 2.86 \pm 0.09$. Constraints have also been placed on the parameters of a number of models which predict deviations from the SM expectations for the single-photon and missing energy, two-photon and missing energy, and hard collinear photon final-state cross sections.

Acknowledgements

References

[1] ALEPH Collaboration, *"Search for supersymmetry in the photon(s) plus missing energy channels at $\sqrt{s} = 161\,GeV$ and $172\,GeV$"*, Phys. Lett. **B420** (1998) 127;
ALEPH Collaboration, *"Single- and multi-photon production in e^+e^- collisions at a centre-of-mass energy of $183\,GeV$"*, Phys. Lett. **B429** (1998) 201.

[2] DELPHI Collaboration, *"Search for pair-produced neutralinos in events with photons and missing energy from e^+e^- collisions at $\sqrt{s} = 130$-$183\,GeV$"*, Eur. Phys. J. **C6** (1999) 371.

[3] L3 Collaboration, *"Single and multi-photon events with missing energy in e^+e^- collisions at $\sqrt{s} = 189\,GeV$"*, Phys. Lett. **B470** (1999) 268;
OPAL Collaboration, *"Photonic Events with Missing Energy in e^+e^- Collisions at $\sqrt{s} = 189\,GeV$"*, Eur. Phys. J. **C18** (2000) 253.

[4] DELPHI Collaboration, *"Determination of the $e^+e^- \to \gamma\gamma(\gamma)$ cross section at centre-of-mass energies ranging from $189\,GeV$ to $202\,GeV$"*, Phys. Lett. **B491** (2000) 67;
L3 Collaboration, *"Study of Multiphoton Final States and Tests of QED in e^+e^- Collisions at $\sqrt{s}$ up to $208\,GeV$"*, Phys. Lett. **B531** (2002) 28;
OPAL Collaboration, *"Multi-photon production in e^+e^- collisions at $\sqrt{s} = 189\,GeV$"*, Phys. Lett. **B465** (1999) 303.

[5] S. Ambrosanio *et al.*, Phys. Rev. **D55** (1997) 1372.

[6] S. Dimopoulos, S. Thomas and J. D. Wells, Nucl. Phys. **B488** (1997) 39.

[7] A. Brignole, F. Feruglio and F. Zwirner, Nucl. Phys. **B516** (1998) 13.

[8] N. Arkani-Hamed, S. Dimopoulos and G. Dvali, Phys. Lett. **B429** (1998) 263.

[9] O. J. P. Eboli *et al.*, Phys. Lett. **B271** (1991) 274.

[10] F. Boudjema, A. Djouadi and J. L. Kneur, Z. Phys. **C57** (1993) 425.

[11] B. Vachon, *"Excited electron contribution to the $e^+e^- \to \gamma\gamma$ cross-section"*, hep-ph/0103132 (2001).

[12] ALEPH Collaboration, *"ALEPH: A detector for electron-positron annihilations at LEP"*, Nucl. Instrum. and Methods **A294** (1990) 121.

[13] ALEPH Collaboration, *"Performance of the ALEPH detector at LEP"*, Nucl. Instrum. and Methods **A360** (1995) 481.

[14] S. Jadach, B. F. L. Ward and Z. Was, Comput. Phys. Commun. **130** (2000) 260.

[15] D. R. Yennie, S. C. Frautschi and H. Suura, Annals of Phys. **13** (1961) 379.

[16] G. Montagna *et al.*, Nucl. Phys. **B541** (1999) 31.

[17] *"Reports of the Working Groups on Precision Calculations for LEP2 Physics"*, Eds. S. Jadach, G. Passarino and R. Pittau, CERN Report 2000-09 (2000) 1.

[18] F. A. Berends and R. Kleiss, Nucl. Phys. **B186** (1981) 22.

[19] P. Janot, *"Tests of QED to O(α^3) and O(α^4) and a search for excited leptons, using the CELLO detector at PETRA"*, Ph.D. Thesis, LAL 87-31 (1987), unpublished.

[20] S. Katsanevas and S. Melachroinos, in *"Physics at LEP2"*, Eds. G. Altarelli, T. Sjöstrand, F. Zwirner, CERN Report 96-01, Volume 2 (1996) 328.

[21] F. A. Berends and R. Kleiss, Nucl. Phys. **B260** (1985) 32.

[22] S. Jadach, W. Placzek and B. F. L. Ward, Phys. Lett. **B390** (1997) 298.

[23] The LEP Collaborations, *"A Combination of Preliminary Electroweak Measurements and Constraints on the Standard Model"*, CERN-EP/2001-098.

[24] J. L. Lopez, D. V. Nanopoulos and A. Zichichi, Phys. Rev. **D55** (1997) 5813.

[25] G. F. Giudice, R. Rattazzi and J. Wells, Nucl. Phys. **B544** (1999) 3 and errata hep-ph/9811291 v2, 13 March 2000, with a change of notation $(1/M_\mathrm{s}^\pm)^4 = -(\pi/2)(1/\Lambda_\mathrm{T}^\pm)^4$.

[26] ALEPH Collaboration, *"Search for Gauge Mediated SUSY Breaking topologies at $\sqrt{s} = 189\,GeV$"*, Eur. Phys. J. **C16** (2000) 71.

[27] S. Dimopoulos, S. Thomas and J. D. Wells, Phys. Rev. **D54** (1996) 3283.

[28] R. D. Cousins and V. L. Highland, Nucl. Instrum. and Methods **A320** (1992) 331.

[29] CDF Collaboration, *"Searches for New Physics in Diphoton Events in $p\bar{p}$ Collisions at $\sqrt{s} = 1.8\,TeV$"*, Phys. Rev. Lett. **81** (1998) 1791 and Phys. Rev. **D59** (1999) 092002.

[30] J. L. Lopez and D. V. Nanopoulos, Phys. Rev. **D55** (1997) 4450.

[31] ALEPH Collaboration, *"Search for Gauge Mediated SUSY Breaking topologies in e^+e^- collisions at centre-of-mass energies up to $209\,GeV$"*, CERN-EP/02-021 (Submitted to Eur. Phys. J. C).
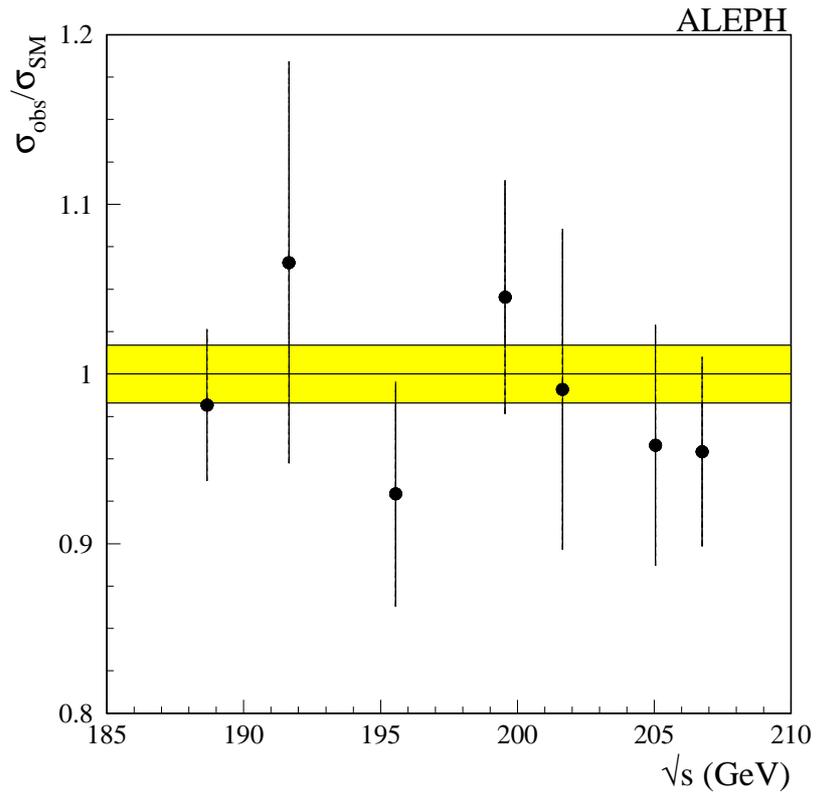
Figure 1: *The ratio of observed to SM cross section as a function of centre-of-mass energy for the process $e^+e^- \rightarrow \nu\bar{\nu}\gamma(\gamma)$. The shaded region represents the common systematic uncertainty of $\pm$ 1.7%.*
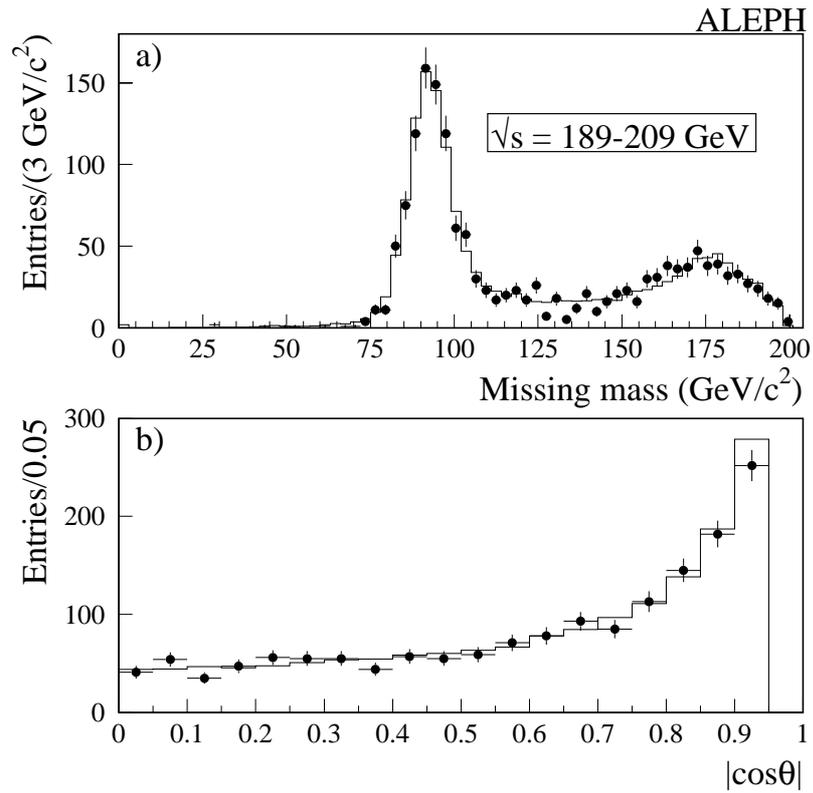
Figure 2: *For the single photon and missing energy sample, the distributions of (a) the invariant mass of the system recoiling against the photon candidate and (b) the photon polar angle, for the data (points with error bars) and the SM expectation (histogram).*
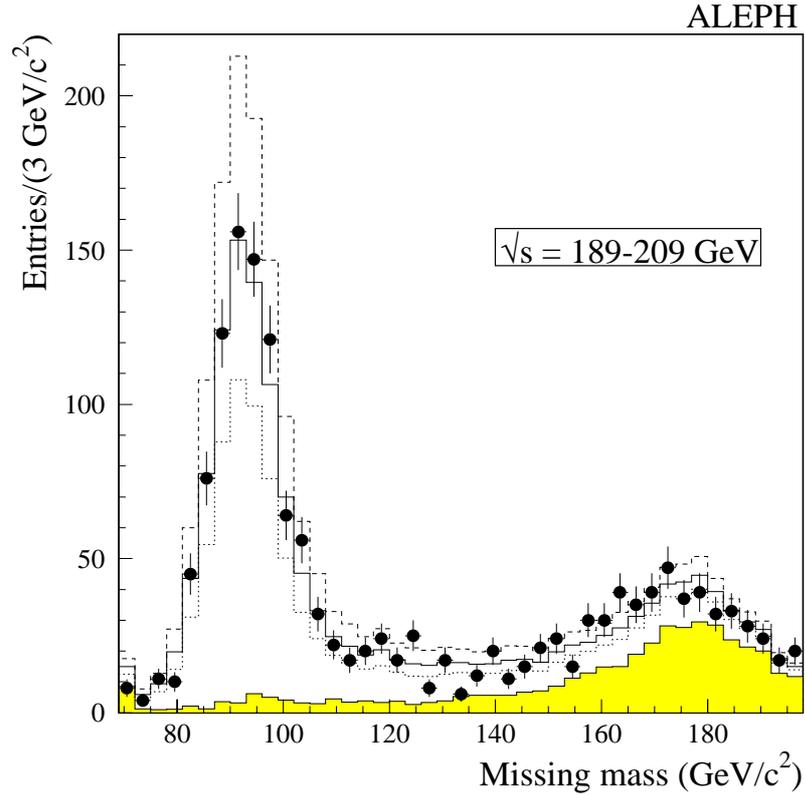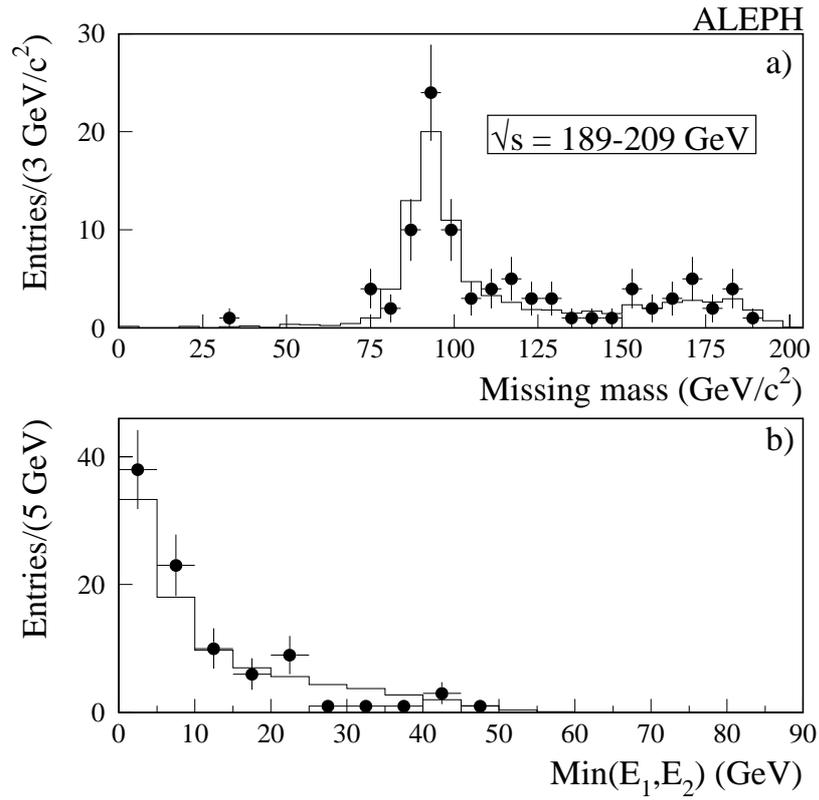
Figure 3: *For the single photon and missing energy sample, the missing mass distribution is shown for the data (points with error bars) and for the prediction of the KK generator for $N_\nu = 2.86$ (solid histogram). Also shown are the expected distributions with $N_\nu = 2$ (dotted histogram) and $N_\nu = 4$ (dashed histogram). The shaded histogram represents the expected contribution from the direct and interference terms due to the t-channel W exchange. The lowest mass bin is treated as an underflow bin.*
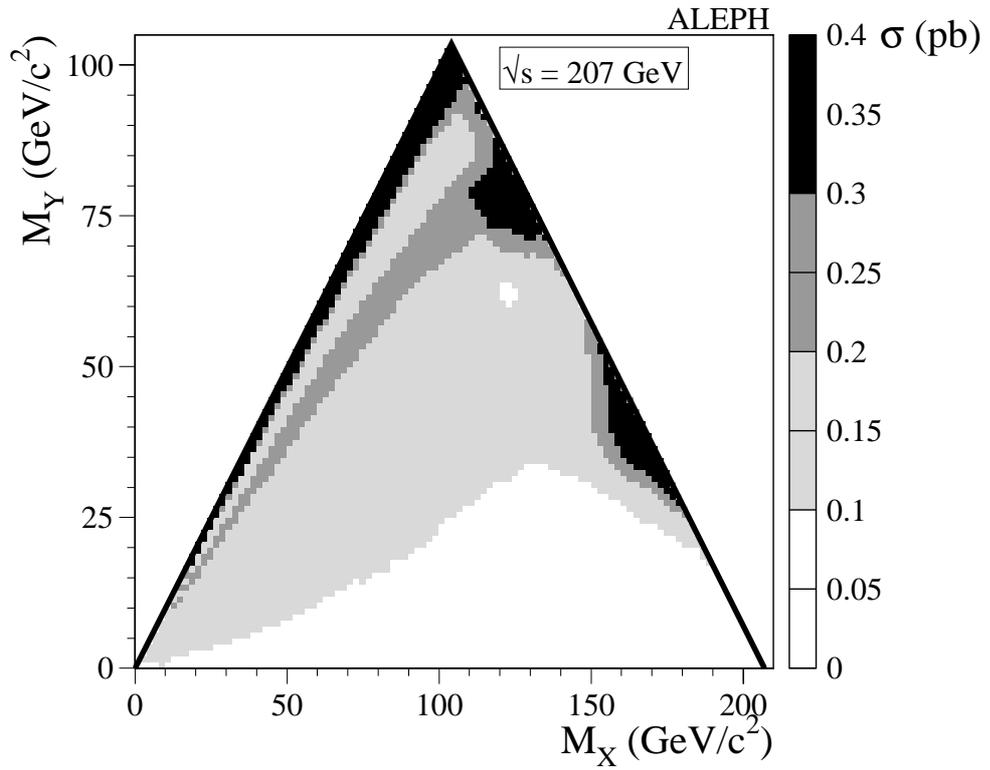
Figure 4: *The 95% C.L. upper limits on the production cross section in pb, valid for* $\sqrt{s} = 207$ *GeV, for the process* $e^+e^- \to XY \to YY\gamma$, *assuming a branching ratio of 100% for* $X \to Y\gamma$.
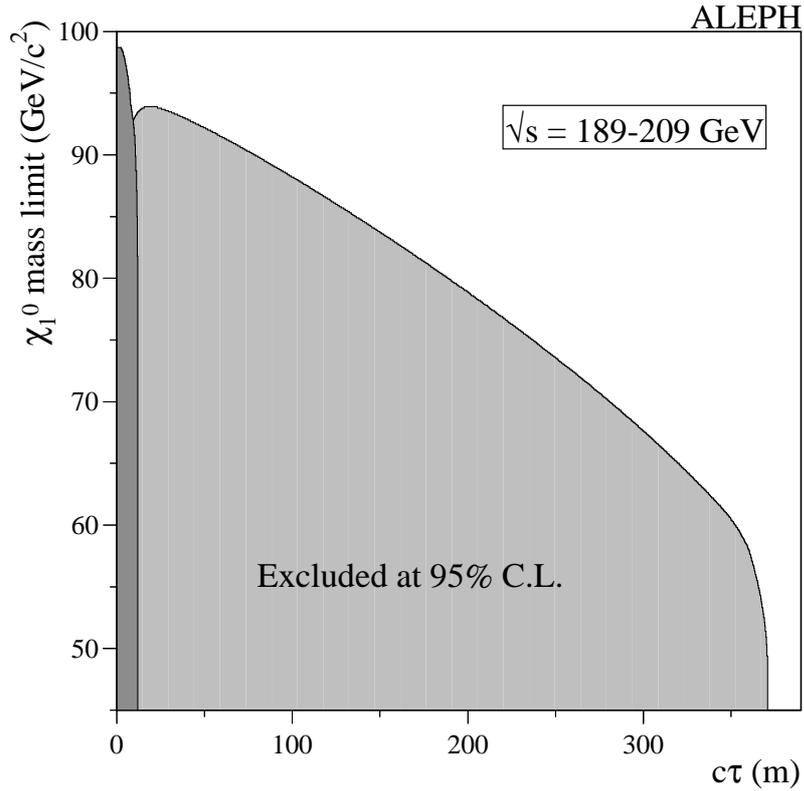
Figure 5: *The excluded regions in the plane of the χ_1^0 mass versus χ_1^0 proper lifetime, at 95% C.L., for the reaction $e^+e^- \to \chi_1^0\chi_1^0 \to \tilde{G}\tilde{G}\gamma\gamma$, under the assumptions of the MGM. The lighter shaded region is based on the search for single photons which do not originate from the interaction region (Section 4.6); the darker shaded region is based on the search for acoplanar photon pairs (Section 5.2).*

Figure 6: *For the two photon and missing energy sample, the distributions of (a) the invariant mass of the system recoiling against the photon candidates and (b) the energy of the second most energetic photon, for the data (points with error bars) and the SM expectation (histogram).*
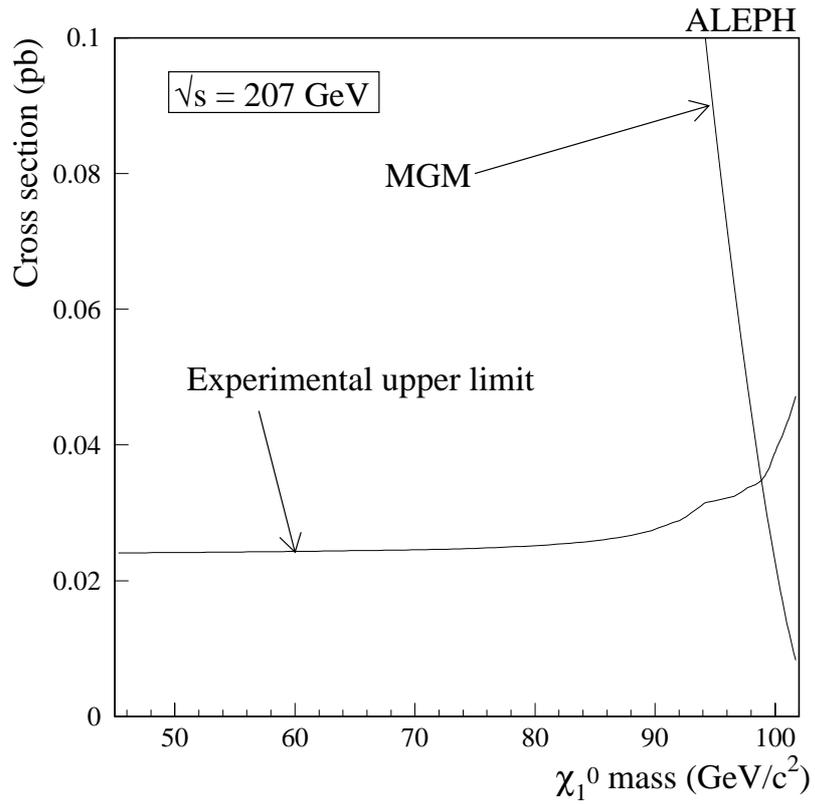
Figure 7: *The 95% C.L. upper limit on the $e^+e^- \rightarrow \chi_1^0\chi_1^0$ cross section, for a $\chi_1^0 \rightarrow \tilde{G}\gamma$ branching ratio of 100% and a small χ_1^0 lifetime ($\tau_{\chi_1^0} < 3\,ns$). Also shown is the expected cross section in the MGM [27].*
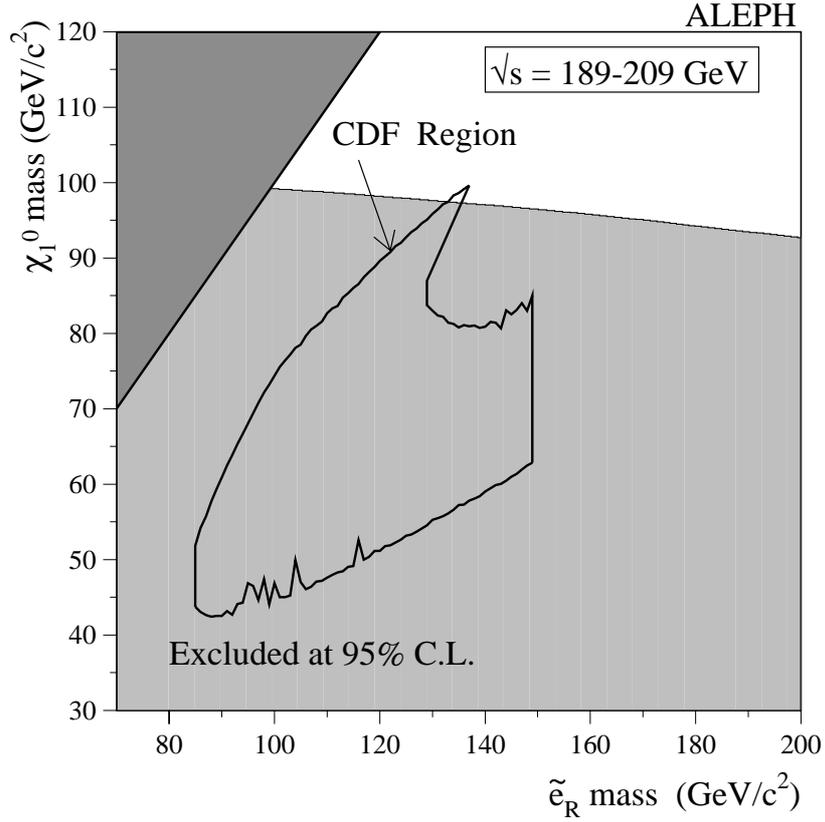
Figure 8: *The excluded region in the neutralino-selectron mass plane at 95% C.L. for the process* $e^+e^- \rightarrow \chi_1^0\chi_1^0 \rightarrow \tilde{G}\tilde{G}\gamma\gamma$ *and a pure bino neutralino (light shaded area). Overlaid is the region favoured by the CDF event [29] assuming the reaction* $q\bar{q} \rightarrow \tilde{e}_R\tilde{e}_R \rightarrow ee\chi_1^0\chi_1^0 \rightarrow ee\tilde{G}\tilde{G}\gamma\gamma$ *[30]. The dark shaded region corresponds to* $M_{\tilde{e}_R} < M_{\chi_1^0}$.
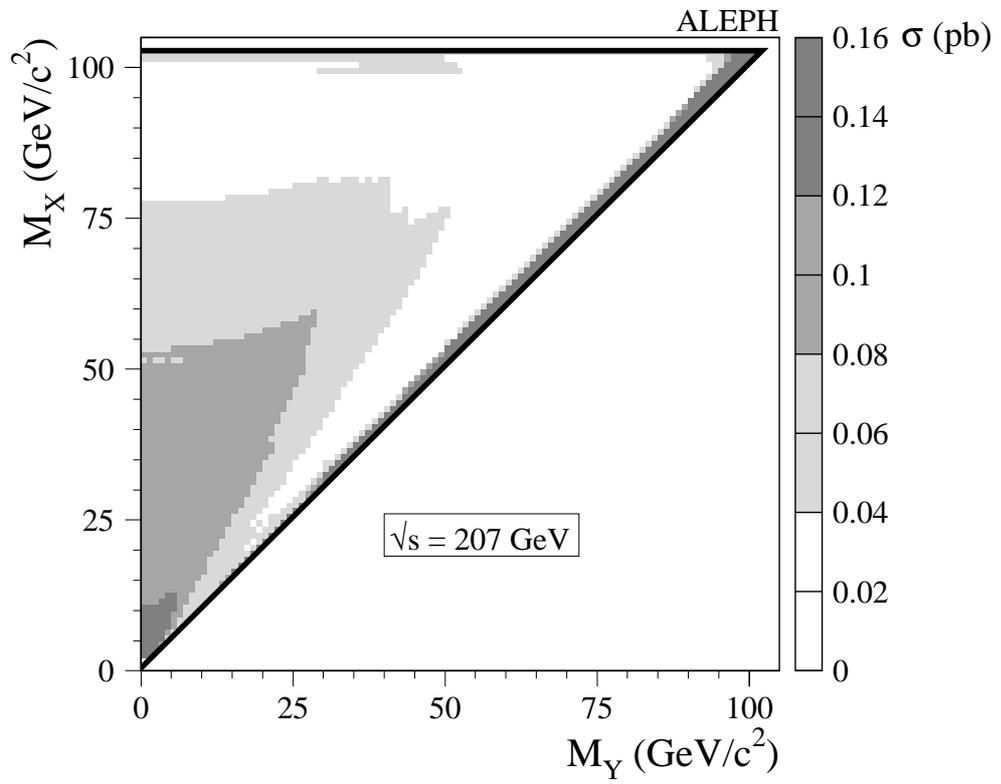
Figure 9: *The 95% C.L. upper limit on the production cross section in pb for the process* $e^+e^- \to XX \to YY\gamma\gamma$ *multiplied by the square of the branching ratio* $\mathcal{B}(X \to Y\gamma)$.
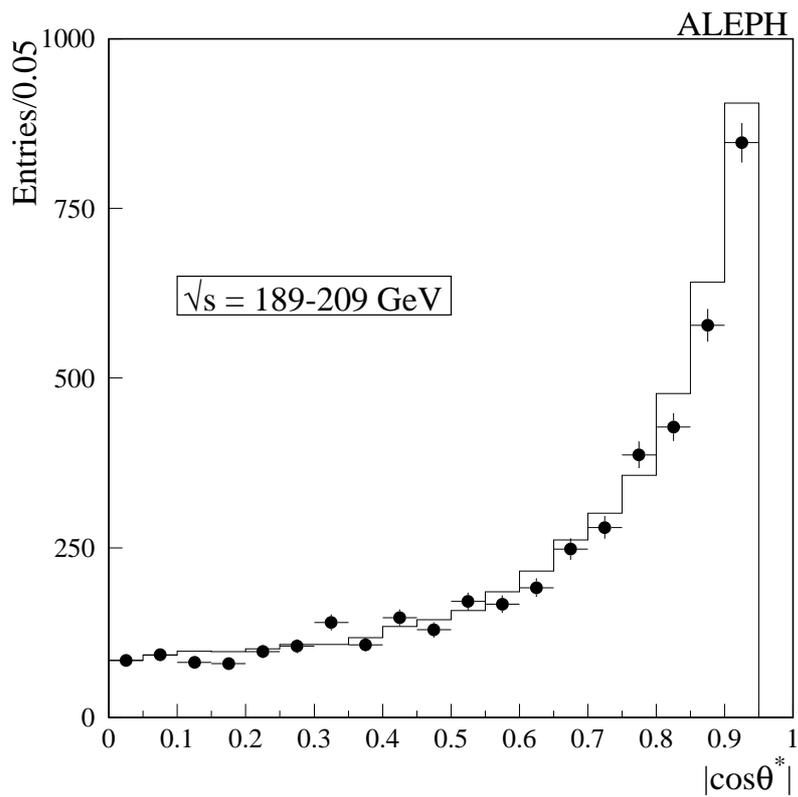
Figure 10: *Predicted (histogram) and observed (points with error bars) angular distributions for the reaction* $e^+e^- \to \gamma\gamma$ *as a function of* $|\cos\theta^*|$, *where* θ^* *is the photon production angle in the two-photon rest frame. The errors shown here are purely statistical.*
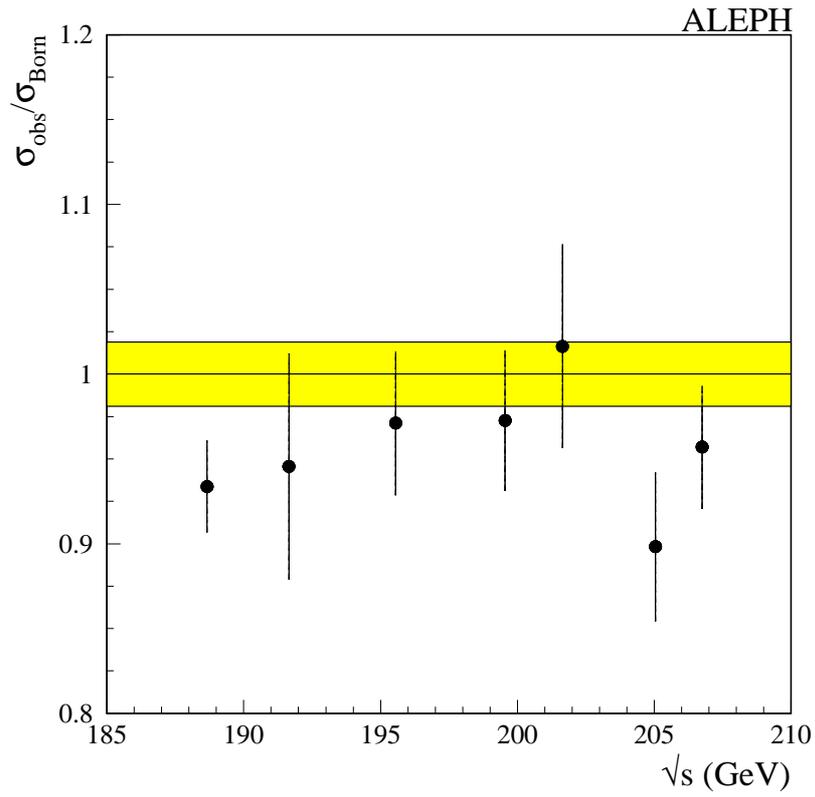
Figure 11: *The ratio of observed to Born cross section as a function of centre-of-mass energy for the process $e^+e^- \rightarrow \gamma\gamma$, for the acceptance region $|\cos\theta^*| < 0.95$. The shaded region represents the common systematic uncertainty of $\pm$ 1.9%.*
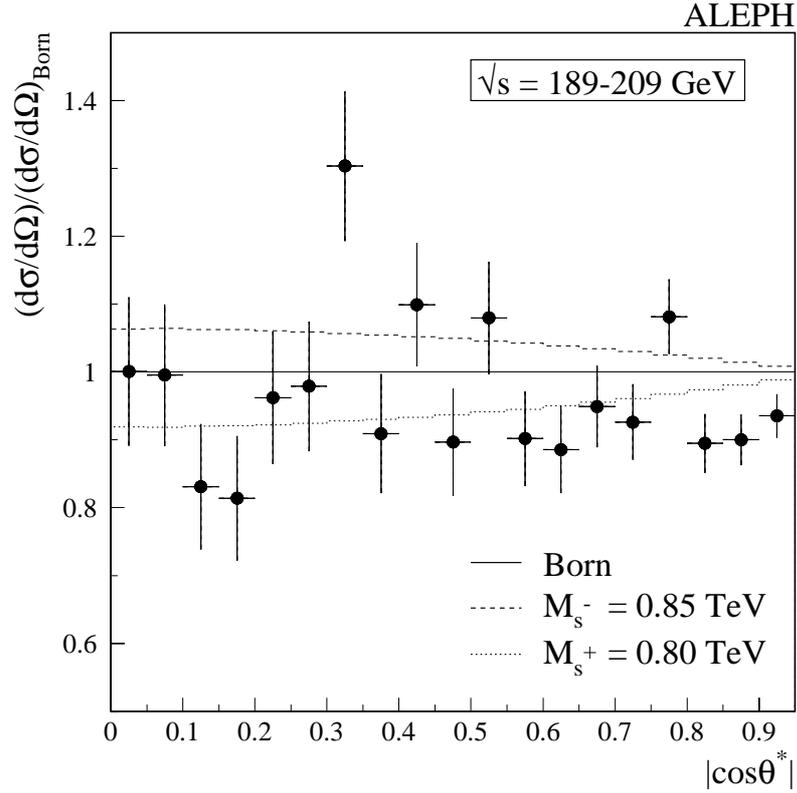
Figure 12: *The ratio of the observed to the predicted differential cross section for* $e^+e^- \to \gamma\gamma$ *as a function of* $|\cos\theta^*|$*, where* θ^* *is the photon production angle in the two-photon rest frame. The dotted and dashed lines correspond to the predictions for virtual graviton exchange, with* M_s^+ *(*M_s^-*) equal to its 95% C.L. lower limit of 0.80 (0.85) TeV.*